Toward the Rational Design of Lipid Gene Vectors: Shape Coupling between Lipoplex and Anionic Cellular Lipids Controls the Phase Evolution of Lipoplexes and the Efficiency of DNA Release

Daniela Pozzi,*,† Giulio Caracciolo,*,† Ruggero Caminiti,† Sofia Candeloro De Sanctis,† Heinz Amenitsch,‡ Cristina Marchini,*,§ Maura Montani,§ and Augusto Amici§

Department of Chemistry, University of Rome "La Sapienza", Piazzale A. Moro 5, 00185 Rome, Italy, Institute of Biophysics and Nanosystems Research, Austrian Academy of Sciences, Schmiedelstrasse 6, A-8042 Graz, Austria, and Genetic Immunization Laboratory, Department of Molecular Cellular and Animal Biology, University of Camerino, Via Gentile III da Varano, 62032 Camerino (MC), Italy

ABSTRACT A viewpoint now emerging is that a critical factor in lipid-mediated transfection (lipofection) is the structural evolution of lipoplexes upon interaction with anionic cellular lipids, resulting in DNA release. At the early stages of interaction, we found a universal behavior of lipoplex/anionic lipid (AL) mixtures: the lipoplex structure is slightly perturbed, while the one-dimensional DNA lattice between cationic membranes is largely diluted by ALs. This finding is in excellent agreement with previous suggestions on the mechanism of DNA unbinding from lipoplexes by ALs. Upon further interaction, the propensity of a given lipoplex structure to be solubilized by anionic cellular lipids strongly depends on the shape coupling between lipoplex and ALs. Furthermore, we investigated the effect of the membrane charge density and a general correlation resulted: the higher the membrane charge density of anionic membranes, the higher their ability to solubilize the structure of lipoplexes and to promote DNA release. Lastly, the formation of nonlamellar phases in lipoplex/AL mixtures is regulated by the propensity of anionic cellular lipids to adopt nonlamellar phases. Remarkably, also phase transition rates and DNA release were found to be strongly affected by the shape coupling between lipoplex and ALs. It thus seems likely that the structural and phase evolution of lipoplexes may only be meaningful in the context of specific anionic cellular membranes. These results highlight the phase properties of the carrier lipid/cellular lipid mixtures as a decisive factor for optimal DNA release and suggest a potential strategy for the rational design of efficient cationic lipid carriers.

KEYWORDS: cationic liposomes • DNA • lipoplexes • cellular lipids • cell transfection • small-angle X-ray scattering • gel electrophoresis

1. INTRODUCTION

Nowadays, synthetic cationic liposomes (CLs) are the most promising nonviral gene vectors (1). When mixed with negatively charged DNA, CLs form stable complexes (lipoplexes) with a well-ordered structure at the nanoscale (Figure 1). During the past decade, the ease of cationic lipid synthesis and the availability of lipid technologies resulted in a huge number of lipid transfection reagents. Most reports have presented data on various cationic lipid chemical structures and also on formulation procedures (2).

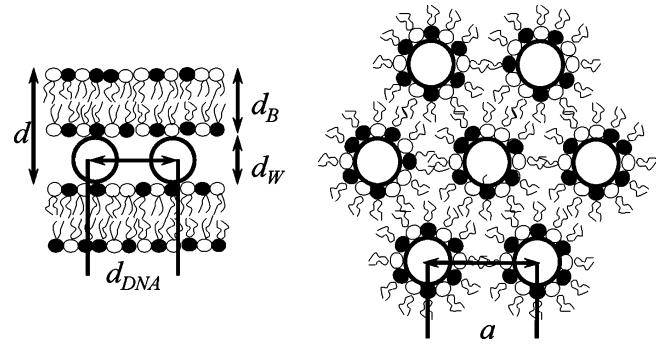

FIGURE 1. Schematic picture of the equilibrium phases of lipoplexes, showing the local structure of their interior on the nanometer scale. Neutral and cationic lipids are depicted as having white and black headgroups, respectively. The lamellar phase, composed of alternative lipid bilayers and DNA monolayers, with a repeat spacing given by $d = d_B + d_W$ is depicted on the left. The hexagonal phase, which consists of DNA coated with a lipid monolayer arranged on a hexagonal lattice, is shown on the right.

Physical−chemical properties of lipoplexes have been deeply investigated both theoretically (3−10) and experimentally (11−25). Unfortunately, the absence of supporting biology resulted in the "plateauing" of transfection efficien-

* To whom correspondence should be addressed. E-mail: d.pozzi@caspur.it (D.P.), g.caracciolo@caspur.it (G.C.), cristina.marchini@unicam.it (C.M.). Tel.: (+39) 06 49913076, (+39) 0737 403276. Fax: (+39) 06 490631, 0737403290.

Received for review June 11, 2009 and accepted September 8, 2009

† University of Rome "La Sapienza".

‡ Austrian Academy of Sciences.

§ University of Camerino.

DOI: 10.1021/am900406b

cies by lipoplexes (26). As a result, a need to elucidate the mechanisms by which nanocarriers mediate functional plasmid DNA delivery in order to incorporate this knowledge into the rational design of cationic lipids is currently more compelling.

A viewpoint now emerging is that a critical factor in the lipid-mediated gene delivery is the structural and phase evolution of lipoplexes upon interaction and mixing with anionic cellular lipids (27−30). Such a structural rearrangement is supposed to play a central role in the DNA escape process, i.e., in how DNA dissociates from lipoplexes and is released into the cytoplasm and, eventually, into the nucleus. A number of recent findings (27−30) seem to support a general conclusion: the greater the tendency of lipoplexes to generate high curvature phases when mixed with anionic lipids (ALs), the larger the DNA release. In earlier publications (31, 32), we examined the interaction between various multicomponent lipoplex formulations and pure anionic membranes but did not find a general correlation between lipoplex phase evolution and DNA release. Thus, this point still remains controversial, and further data are urgently needed to generalize the results.

According to the present understanding, the very first interaction between lipoplexes and biomembranes is largely dominated by electrostatics. Thus, charge densities of lipoplexes and anionic membranes are expected to play a key role in membrane interaction, contact, fusion, and DNA release (27−32). Specifically, whether the membrane charge density of anionic membranes plays a role in the DNA release process and to what extent the phase evolution of lipoplexes does depend on the intrinsic curvature of anionic cellular membranes have yet to be deeply understood. In order to extend the previous research, here we used pure ALs, lipid mixtures similar to real membranes, and lipid extracts from mammalian tissues. The structural and phase evolution of lipoplexes were investigated by synchrotron small-angle X-ray scattering (SAXS), while DNA release was determined by gel electrophoresis (33). We provide the following body of evidence: (i) the ranking of lipoplexes with respect to their propensity to be solubilized by ALs is strongly dependent on the shape coupling between of lipoplex and cellular lipids; (ii) the same principle regulates the distinction of ALs between strong and weak DNA releases; (iii) the higher the membrane charge density of anionic membranes, the higher their ability to solubilize the structure of lipoplexes and to promote DNA release; (iv) the phase behavior of lipoplex/AL mixtures is largely dependent on the cellular lipid species. It thus seems likely that the structural and phase evolution of lipoplexes may only be meaningful in the context of specific anionic membranes. These results highlight the phase properties of the carrier lipid/cellular lipid mixtures as a decisive factor for optimal DNA release and suggest a potential strategy for the rational design of efficient cationic lipid carriers.

2. MATERIALS AND EXPERIMENTAL METHODS

2.1. CL Preparation. Cationic 1,2-dioleoyl-3-trimethylammonium propane (DOTAP) and [3β-[*N*-[(*N*′,*N*′-dimethylamino)-ethyl]carbamoyl]]cholesterol (DC-Chol) and neutral dioleoylphosphatidylethanolamine (DOPE), dioleoylphosphocholine (DOPC), 1,2-dilauroyl-*sn*-glycero-3-phosphocholine (DLPC), and 1,2-dimyristoyl-*sn*-glycero-3-phosphocholine (DMPC) were purchased from Avanti Polar Lipids (Alabaster, AL) and used without further purification. DOTAP−DOPC, DOTAP−DLPC, DOTAP−DOPE, DC-Chol−DOPE, and DC-Chol−DMPC CLs were prepared according to standard protocols (34). In brief, binary mixtures, at molar fractions of neutral lipid in the bilayer Φ = (neutral lipid/total lipid) (mol/mol) = 0.25 and 0.5, were dissolved in chloroform, and the solvent was evaporated under vacuum for at least 24 h. The obtained lipid films were hydrated with the appropriate amount of a Tris-HCl buffer solution (10^{-2} M, pH 7.4) to achieve the desired final concentration (10 and 1 mg/mL for SAXS and electrophoresis experiments, respectively). The obtained liposome solutions were stored at 30 °C for 24 h to achieve full hydration. Indeed, we have recently found evidence that lipid hydration is important to achieving the equilibrium structure of lipoplexes (34).

2.2. AL Preparation. Anionic dioleoylphosphatidylglycerol (DOPG), dioleoylphosphatidic acid (DOPA), and dioleoylphosphatidylserine (DOPS) were purchased from Avanti Polar Lipids (Alabaster, AL) and used without further purification. The protocol described in section 2.1 was followed to prepare anionic liposomes made of DOPG, DOPA, and DOPS. Negatively charged liposomes mimicking membrane (MM) were also prepared [MM1 = DOPC:DOPE:DOPG (33:33:33, w/w); MM2 = DOPC:DMPC:DOPE:DOPS (26:26:27:21, w/w)]. The lipid concentration was 10 mg/mL for X-ray samples and was lowered to 1 mg/mL for electrophoresis experiments.

2.3. Natural Lipid Extracts. Polar lipid extracts from bovine liver were purchased from Avanti Polar Lipids (Alabaster, AL) and used without further purification. ALs made of liver polar extracts (LPEs) were prepared according to the protocol described in section 2.1.

2.4. Lipoplex Preparation. For SAXS measurements, calf thymus (CT) Na-DNA, purchased from Sigma-Aldrich (St. Louis, MO), was used. For electrophoresis experiments, plasmid DNA, purchased from Promega (Madison, WI), was employed. CT Na-DNA was dissolved in a Tris-HCl buffer (5 mg/mL) and was sonicated for 5 min, inducing a DNA fragmentation with length distribution between 500 and 1000 base pairs, which was determined by gel electrophoresis. By mixing adequate amounts of the DNA solutions to suitable volumes of liposome dispersions, self-assembled DOTAP−DOPC/DNA, DOTAP−DLPC/DNA, DOTAP−DOPE/DNA, DC-Chol−DOPE/DNA, DC-Chol−DMPC/DNA, DC-Chol−DMPC−DOPE/DNA binary lipoplexes were obtained. Multicomponent lipoplexes, incorporating three or four lipid species, were prepared by adding DNA to mixed lipid dispersions made of distinct populations of CLs (35−37). All samples were prepared at room temperature with the same cationic lipid/DNA ratio (mol/mol), i.e., ρ = cationic lipid (by mole)/DNA base = 3.2. The chosen charge ratio (positively charged lipoplexes) guarantees a maximum DNA load, which is not always the case for isoelectric complexes (ρ = 1) (38). Complexes were prepared at room temperature and were allowed to equilibrate for 30 min before use. Upon mixing, lipoplexes immediately formed and no vortexing was needed.

2.5. Lipoplex/Anionic Liposome System Preparation. Lipoplexes and ALs made of DOPG, DOPS, DOPA, MM1, MM2, and LPE liposomes were mixed at different anionic/cationic charge ratios R = 0, 0.1, 0.2, 0.5, 1, 2, 3, 4, 5, 7, 8, 9, 10, 15, 20, and 25. These mixed dispersions were then equilibrated for 2 days. To ensure equilibration, the samples were kept at 4 °C for 2 days. As previous kinetic experiments demonstrated, to reach equilibrium, 2 days is more than sufficient (39).

2.6. Synchrotron SAXS Measurements. X-ray measurements were partly performed at the Austrian SAXS station of the synchrotron light source ELETTRA (Trieste, Italy) (40). SAXS

patterns were recorded with two gas detectors based on the delay line principle covering q ranges. We investigated the q range from $q_{min} = 0.05$ Å^{-1} to $q_{max} = 0.6$ Å^{-1} with a resolution of 5×10^{-4} Å^{-1} (fwhm). The angular calibration of the detectors was performed with silver behenate powder (d spacing = 58.38 Å). The sample was held in a 1 mm glass capillary (Hildberg, Germany). The data have been normalized for variations of the primary beam intensity, corrected for the detector efficiency, and the background has been subtracted. Measurements were performed at 25 °C. The temperature was controlled in the vicinity of the capillary to within ±0.1 °C (Anton Paar, Graz, Austria). Exposure times were typically 300 s. No evidence of radiation damage was observed in the X-ray diffraction patterns.

SAXS measurements were carried out also at the ID2 high-brilliance beamline at the European Synchrotron Radiation Facility (Grenoble, France). The energy of the incident beam was 12.5 keV ($\lambda = 0.995$ Å), the beam size was 100 μm, and the sample-to-detector distance was 1.2 m. The diffraction patterns were collected with a two-dimensional (2D) CCD detector (Frelon Camera). We investigated the q range from $q_{min} = 0.04$ Å^{-1} to $q_{max} = 0.5$ Å^{-1} with a resolution of 5×10^{-4} Å^{-1} (fwhm). The sample was held in a 1 mm glass capillary (Hildberg, Germany). Measurements were performed at 25 °C. To avoid radiation damage, a maximum exposure time of 3 s frame^{-1} was used for any given sample. Satisfactory statistics were obtained by repeating several measurements on fresh samples. The collected 2D powder diffraction spectra were angularly integrated as described elsewhere (41). These data were then corrected for the detector efficiency, empty sample holder, and bulk solution.

2.7. Agarose Gel Electrophoresis Experiments. Electrophoresis studies were conducted on 1% agarose gels containing a Tris-Borate-EDTA (TBE) buffer. After electrophoresis, ethidium bromide was added and then visualized. Lipoplexes were prepared by mixing 20 μL of lipid dispersions (1 mg/mL, a Tris-HCl buffer) with 5 μg of pGL3 control plasmid. These complexes were allowed to equilibrate for 3 days at 4 °C before the addition of negatively charged liposomes. After 24 h, naked plasmid DNA, lipoplexes, and lipoplexes/ALs systems with different R values were analyzed by electrophoresis. For this purpose, 10 μL of each sample was mixed with 2 μL of a loading buffer [glycerol 30% (v/v) and bromophenol blue 0.25% (v/v)] and subjected to agarose gel electrophoresis for 1 h at 80 V. The electrophoresis gel was visualized and digitally photographed using a Kodak Image Station, model 2000 R (Kodak, Rochester, NY). Digital photographs were elaborated using a dedicated software (Kodak MI, Kodak) that allows calculation of the molar fraction of released DNA, X_{DNA}.

3. RESULTS

3.1. SAXS Experiments. In an effort to rationalize the effect of ALs on the structure and phase behavior of lipoplexes, we performed a comprehensive synchrotron SAXS study on lipoplex/AL mixtures as a function of the anionic/cationic charge ratio, R.

3.1.1. Structural Changes of Lipoplexes upon Interaction with ALs. Figure 2 shows representative SAXS patterns of lipoplexes ($\Phi = 0.5$) at $R = 0$ (no AL added). The sharp peaks labeled at q_{00l} arose from the lamellar periodicity along the normal to the lipid bilayer, d, which is the sum of the membrane thickness (d_B) and the thickness of the water/DNA layer (d_W): $d = d_B + d_W = 2\pi/q_{001}$ (Figure 1). The diffuse broader peak (marked by an arrow) resulted from one-dimensional (1D) in-plane packing of the intercalated DNA strands, which form a 1D-ordered

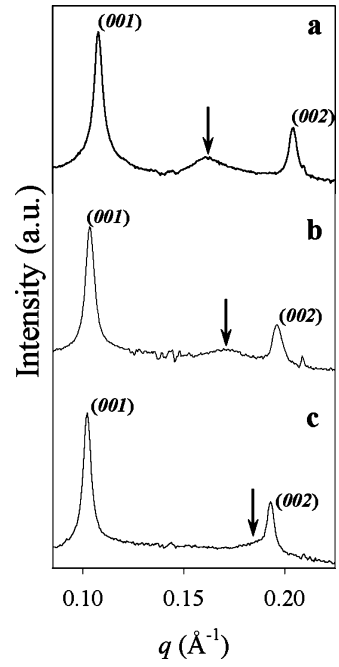

FIGURE 2. Representative synchrotron SAXS patterns: DOTAP−DOPC/DNA (a); DOTAP−DC-Chol−DOPC−DOPE/DNA (b); DC-Chol−DOPE−DMPC/DNA (c). The sharp peaks labeled at q_{00l} arose from the lamellar periodicity along the normal to the lipid bilayer, d, which is the sum of the membrane thickness (d_B) and the thickness of the water/DNA layer (d_W): $d = d_B + d_W$. The DNA−DNA mobile peak is marked by an arrow.

array with a characteristic interaxial spacing, $d_{DNA} = 2\pi/q_{DNA}$ (Figure 1). It is worth mentioning that each SAXS pattern arose from a single lamellar phase with characteristic lamellar d spacing and DNA packing density.

After the addition of negatively charged DOPG to preformed lipoplexes, the structural organization of the membranes changed remarkably. Figure 3 shows representative SAXS patterns of DOTAP−DLPC/DNA/DOPG mixtures in the $0 < R < 0.5$ range of the anionic/cationic charge ratio. Note that the lamellar repeat distance, d, did not change significantly as a function of R ($d = 62$ and 64.5 Å at $R = 0$ and 0.5, respectively), therefore suggesting that DNA remained tightly bound to lipid bilayers (31). However, a direct comparison of the diffraction patterns of Figure 3 shows that a decrease in the height is also accompanied by a progressive broadening of diffraction peaks as a function of increasing R. Because the full width at half-maximum (fwhm) of a diffraction peak is related, among other things, to the size of the domains from which the diffraction comes, the latter observation is likely to mean that anionic DOPG perturbed the long-range order of the lipoplex structure. The average domain size of the multilayers and the DNA arrays, L_m, was estimated using the Debye−Scherrer relation $L_m = 2\pi/\Delta q$, where Δq is the fwhm of the (001) diffraction peak in q space. For the calculation, we used $\Delta q = [(\text{fwhm})_{exp}^2 - (\text{fwhm})_{beam}^2]^{1/2}$, where $(\text{fwhm})_{exp}$ is the experimental width of the (001) diffraction peak and $(\text{fwhm})_{beam}$ is the width of the intrinsic instrumental resolution function [$(\text{fwhm})_{beam} \sim 6 \times 10^{-4}$ Å^{-1}]. We have determined that L_m is about 2500 Å with no AL added ($R = 0$), and this value is comparable to those of other cationic lipid/DNA complexes (42). A signifi-

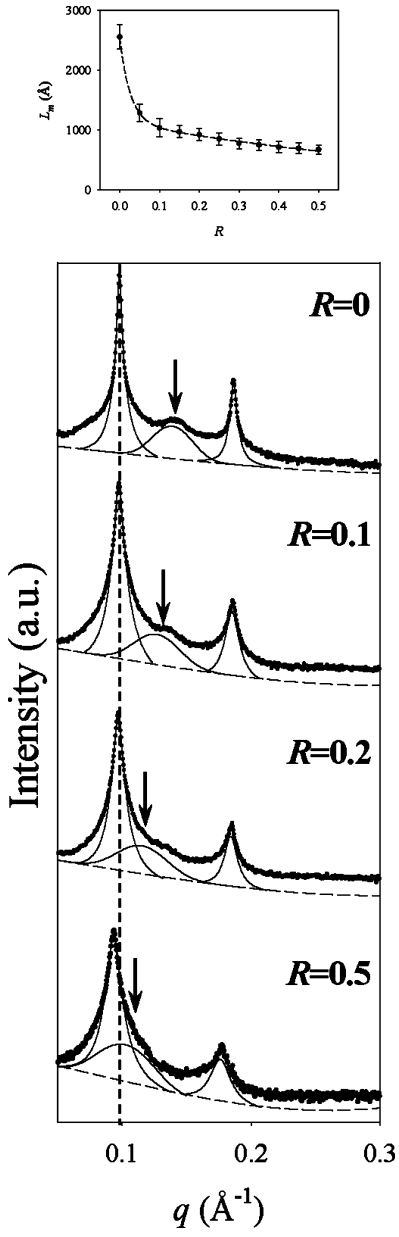

FIGURE 3. SAXS patterns of DOTAP−DLPC/DNA/DOPG mixtures in the $0 < R < 0.5$ range of the anionic/cationic charge ratio. While the position of (00*l*) Bragg peaks changed slightly with *R*, the fwhm changed remarkably, suggesting that DOPG promoted the loss of long-range order along the normal to lipid bilayers. The DNA−DNA distance, d_{DNA}, increased remarkably, as shown by the shift of the DNA peak (marked by an arrow). This indicates that the 1D DNA in-plane rod lattice was progressively diluted by DOPG. The dashed lines are the backgrounds, and the solid lines show the best-fitting functions to diffraction peaks. In the top panel, the change in the average domain size of the multilayers and the DNA arrays, L_m, with *R* is reported.

cant dependence of the average multilayer domain size, L_m, with *R* was found (Figure 3, top panel), suggesting that ALs gradually destabilize the multilamellar nanostructure of lipoplexes.

On the other hand, Figure 3 also shows that the "DNA peak" (vertical arrows) shifted over a wide *q* range, corresponding to a change in d_{DNA} from 38.6 Å ($R = 0$) to 53 Å ($R = 0.5$). This finding indicated that the 1D in-plane rod DNA lattice was diluted by ALs (8). For $R > 0.5$, the DNA peak was

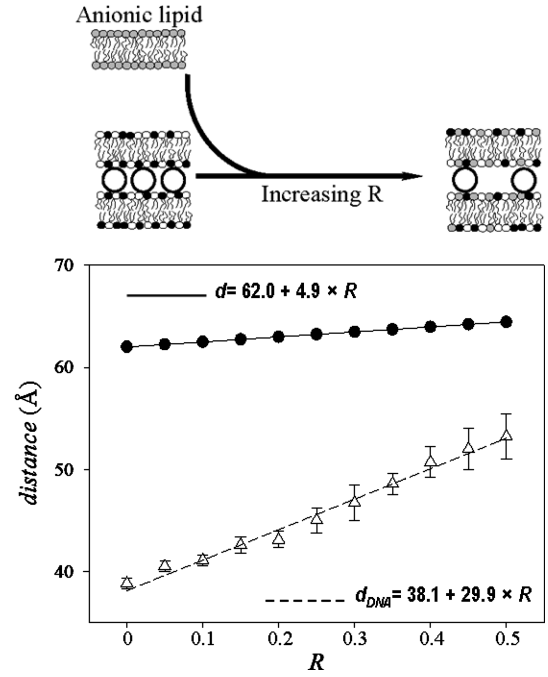

FIGURE 4. Lamellar repeat spacing (black circles) and DNA−DNA interdistance (white triangles), a function of *R*. Solid and dashed lines are the best linear fits to the data (correlation coefficients $r = 0.999$ and 0.973, respectively). The top sketch shows the effect of ALs on the nanometric structure of lipoplexes at low *R*. ALs induce a slight swelling of the lamellar *d* spacing and a major dilution of the 1D DNA lattice.

Table 1. R^{DNA} Is the Value of the Anionic/Cationic Charge Ratio, *R*, at Which DNA−DNA Short-Range Correlation Is Lost, While at $R = R^*$, the Structure of Lipoplexes Is Completely Destroyed by DOPG Molecules

lipoplex	R^{DNA}	R^*
DOTAP−DOPC	0.5	4−5
DOTAP−DLPC	1	5
DOTAP−DOPE	0.5−1	6
DC-Chol−DOPE	0.5−1	12
DC-Chol−DMPC	1	25
DC-Chol−DOPE−DMPC	1	20
DOTAP−DOPC−DC-Chol−DOPE	0.5	8

not detected on the X-ray pattern, suggesting that the increasing amount of AL may perturb the 1D DNA packing. In what follows, we define R^{DNA} as the anionic/cationic charge ratio at which the initial lamellar structure of lipoplexes is almost unperturbed but short-range order in the DNA−DNA correlations is completely lost, as revealed by the disappearance of the "DNA peak" on the SAXS pattern. The phenomenology described (Figure 4) appeared to be absolutely general, but any of the seven lipoplex formulations exhibited a proper R^{DNA} value (Table 1). Because the DNA peak is not well resolved at high *R*, we underline that the linear relationship reported in Figure 4 may be affected by the fitting procedure. However, what is certainly unquestionable is that the DNA lattice is progressively diluted (i.e., d_{DNA} increases) by the insertion of ALs within lipoplex membranes.

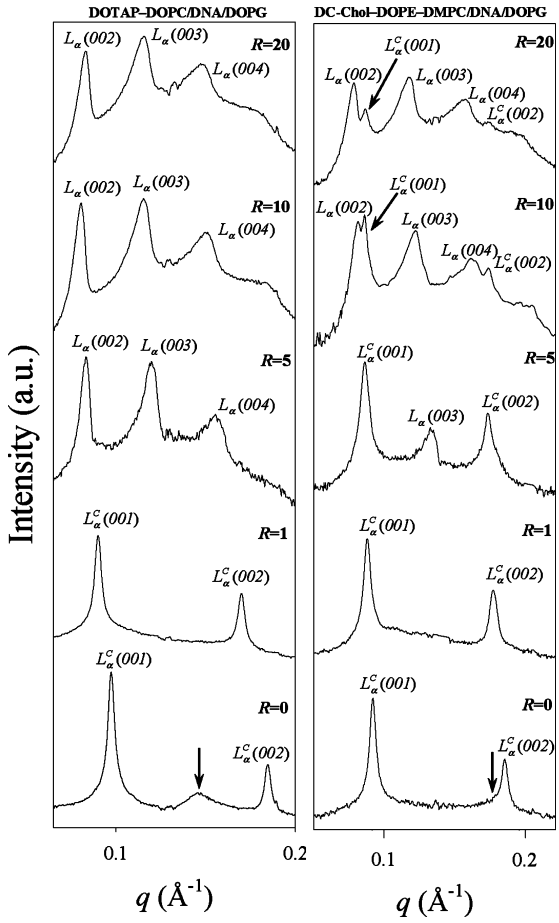

FIGURE 5. SAXS patterns of DOTAP−DOPC/DNA (left panel) and DC-Chol−DOPE−DMPC/DNA (right panel) lipoplexes as a function of the increasing anionic/cationic charge ratio, *R*. At $R = 1$, the structure of lipoplexes resists solubilization, but short-range order in the DNA−DNA correlations is completely lost, as revealed by vanishing of the "DNA peak". At $R = 1$, the lamellar phase starts being destroyed by anionic DOPG. At $R > 5$, only the lamellar phase of pure DOPG appears in the pattern of the DOTAP−DOPC/DNA/DOPG mixture, while DC-Chol−DOPE−DMPC/DNA lipoplexese were found to be much more resistant to disintegration by ALs. Indeed, at $R = 20$, traces of the starting lamellar phase can be seen.

Upon the addition of further DOPG, a major reorganization of the initial multilamellar structure of lipoplexes was observed. Figure 5 shows typical SAXS patterns of two different lipoplex formulations (left panel, DOTAP−DOPC/DNA; right panel, DC-Chol−DOPE−DMPC/DNA) ($\Phi = 0.5$) as a function of *R*. We chose to present these data because these lipid formulations provided the clearest evidence of structural differences upon interaction with anionic DOPG. At $R = 1$, the lamellar phase of DOTAP−DOPC/DNA lipoplexes was still preserved, while at $R = 5$, disintegration was complete. For $R > 5$, the mixed system was identified as being in the swollen liquid-crystalline lamellar phase of pure DOPG ($d = 131.2$ Å). On the other hand, DC-Chol−DOPE−DMPC/DNA/DOPG complexes were much more resistant than DOTAP−DOPC/DNA complexes. Indeed, at $R = 20$, the lamellar DC-Chol−DOPE−DMPC/DNA complexes still resisted disintegration by DOPG, as shown by the presence of the (001) (indicated by an arrow) and (002) Bragg reflections.

In summary, the addition of DOPG to lipoplexes resulted in two different stages that can be summarized as follows. In the first stage, which we called "the DNA lattice dilution regime" ($0 < R < R^{DNA}$), the lamellar structure of lipoplexes is essentially preserved with some changes in the lamellar *d* spacing and in the long-range order. In this regime, the DNA lattice strongly diluted by ALs up to the inter-DNA correlation is completely lost and the DNA peak is no longer observed in the SAXS pattern. In the second regime ($R^{DNA} < R < R^*$), the lipoplex/AL mixture undergoes a remarkable structural change, finally resulting in the complete disintegration of the lamellar phase of lipoplexes.

Most importantly, our results point out the existence of a strict correlation between lipoplex formulations and their propensity to be disintegrated by anionic DOPG. In particular, although the structural behavior was common to all lipoplex/AL mixtures, any of them exhibited highly specific R^{DNA} and R^* values (Table 1).

3.1.2. Effect of the Membrane Charge Density of Anionic Liposomes on the Disintegration of the Lipoplex Structure. To better simulate the conditions that exist when lipoplexes interact with cellular lipids, we used a MM lipid blend, MM1 [DOPC:DOPE:DOPG, 33:33:33 (w/w)], and compared the results with those obtained with pure DOPG. Such a comparison was also expected to elucidate the role of the membrane charge density of anionic membranes on their ability to destabilize the nanostructure of lipoplexes.

Figures 5 (left panel) and 6 together show comparisons between SAXS patterns of DOTAP−DOPC/DNA/DOPG and DOTAP−DOPC/DNA/MM1 systems at increasing *R* values. Lipoplexes/MM1 mixed systems retained their lamellar structure for longer than did lipoplex/DOPG mixtures. For example, at $R = 1$, the DNA peak was not detected on the SAXS pattern of DOTAP−DOPC/DNA/DOPG lipoplexes, whereas it was still present on that of DOTAP−DOPC/DNA/MM1 ones (indicated by an arrow). At $R = 5$, DOTAP−DOPC/DNA lipoplexes were completely disintegrated by pure DOPG, while they partly resisted disintegration when mixed with MM1.

As a general rule, disintegration of lipoplexes by MM1 liposomes occurred at higher R^* values than those needed when using pure DOPG liposomes. SAXS experiments performed using the other six formulations gave comparable results (here not reported for space consideration).

To generalize the results, a second couple of anionic membranes with the same anionic component (DOPS) but a different membrane charge density were used: pure DOPS and MM2 [DOPC:DMPC:DOPE:DOPS, 26:26:27:21 (w/w)]. Figure 7 shows the comparison between the SAXS patterns of the DOTAP−DOPC/DNA/DOPS (left panel) and DOTAP−DOPC/DNA/MM2 (right panel) systems. At $R = 5$, disintegration of DOTAP−DOPC/DNA lipoplexes by DOPS was almost complete, while DOTAP−DOPC/DNA/MM2 mixtures preserve their lamellar arrangement. Indeed, residual Bragg peaks were superimposed to the scattering signal because of the form factor of pure uncorrelated MM2 bilayers. At $R = 10$,

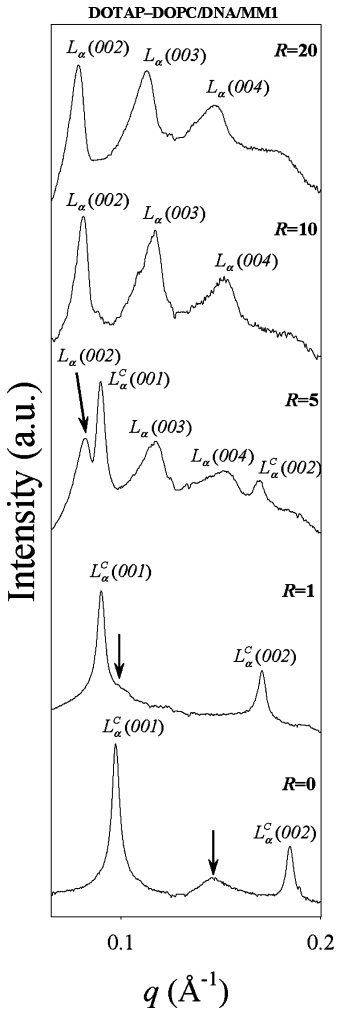

FIGURE 6. SAXS patterns of DOTAP−DOPC/DNA/MM1 mixed systems as a function of increasing anionic/cationic charge ratio, *R*.

DOTAP−DOPC/DNA lipoplexes were completely disintegrated by DOPS (the scattering profile arising from the form factor of uncorrelated DOPS membranes), while they partly resisted solubilization by MM2.

As is evident, these results are in good agreement with those obtained with pure DOPG and MM1 ALs. These findings suggest, therefore, the existence of a strict correlation between the charge density of membranes containing a specific AL species (such as DOPG or DOPS) and their ability to destabilize the structure of lamellar lipoplexes: the higher the charge density of anionic membranes, the higher their ability to solubilize the nanostructure of a given lipoplex formulation.

3.1.3. Phase Evolution of Lipoplexes upon Interaction with ALs with a Propensity To Form Nonlamellar Phases. The anionic membrane lipids DOPS and DOPG are known to be lamellar-phase-forming. To investigate the insurgence of nonlamellar motifs in lipoplex/AL mixtures, DOPA, well-known for its nonlamellar phase tendency, was used. Figure 8 shows the SAXS patterns of DOTAP−DOPC/DNA/DOPA mixtures ($\Phi = 0.5$) as a function of *R*. According to the results discussed in section 3.1.1, SAXS patterns allowed us to identify the extension of the "DNA lattice dilution regime" of DOTAP−DOPC/DNA/DOPA mixtures as being comprised between $R = 0$ and $R^{DNA} = 0.5$. SAXS scans show that d_{DNA} changed from 38.6 Å at $R = 0$ up to about 41.9 Å at $R^{DNA} = 0.5$. As the DOPA concentration was increased in the mixture, a lamellar−hexagonal phase transition occurred. At $R = 0.5$, the diffraction pattern is still dominated by lamellar peaks, but we also observed three Bragg peaks that are indexed as the (10), (11), and (20) reflections of an inverted hexagonal phase with a 71.3 Å structural unit. The initial lamellar phase of DOTAP−DOPC/DNA lipoplexes persisted up to $R \sim 2$. For $R > 2$, the SAXS patterns of the DOTAP−DOPC/DNA/DOPA mixture are dominated by a hexagonal phase, with a unit cell of 75.5 Å. Hexagonal complexes were found to coexist with pure DOPA (bicontinuous cubic phase *Pn*3*m* with a structural unit $a = 150$ Å) until solubilization was completed at $R^* \sim 10$ (not reported). We observe that such a value is about twice as large as that obtained with DOPG ($R^* \sim 5$). This finding suggests that the solubilization ability of anionic membranes depends not only on the molar anionic/cationic ratio, *R*, but also on the specific anionic species.

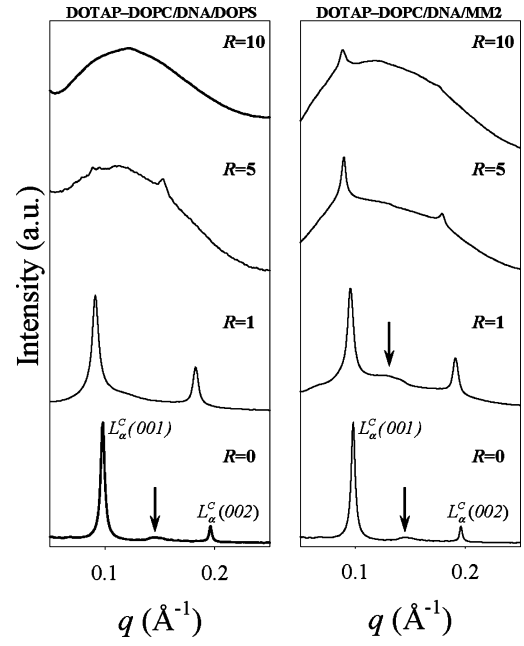

FIGURE 7. SAXS patterns of DOTAP−DOPC/DNA/DOPS and DOTAP−DOPC/DNA/MM2 mixed systems as a function of increasing anionic/cationic charge ratio, *R*. At $R = 5$, it is almost completely destroyed by anionic DOPS and residual Bragg peaks are superimposed to the scattering signal arising from the form factor of uncorrelated DOPS lamellae. As is evident, solubilization of lipoplexes occurred at higher values of *R* when MM2 anionic liposomes were used.

To elucidate the role played by the membrane charge density of lipoplexes in the phase evolution of lipoplex/AL mixtures, lipoplexes of higher membrane charge density were employed. Figure 9 (panel A) shows the comparison between DOTAP−DOPC/DNA/DOPA (left) and DC-Chol−DOPE/DNA/DOPA (right) mixtures ($\Phi = 0.25$) as a function of the anionic/cationic charge ratio *R*. The chosen formulations showed the clearest structural difference, while the other lipoplex/DOPA mixtures exhibited an intermediate behavior (not reported). As the DOPA concentration was increased in the mixture, a lamellar−hexagonal phase transition occurred. At $R = 1$, three Bragg peaks (indicated with white

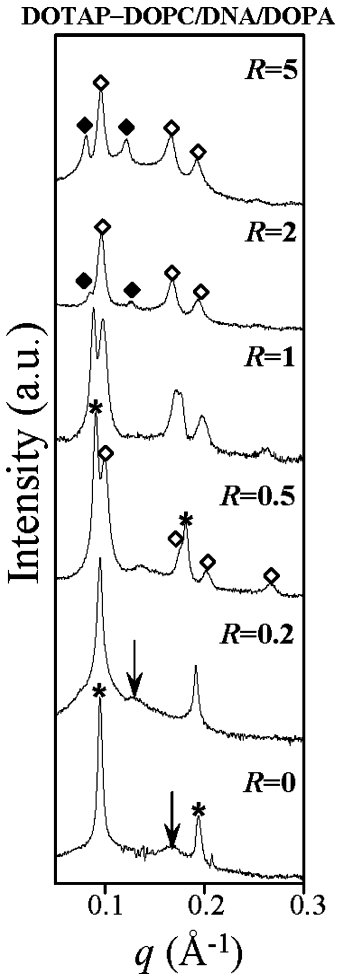

FIGURE 8. SAXS patterns of DOTAP−DOPC/DNA/DOPA mixtures as a function of the anionic/cationic charge ratio *R*. Bragg peaks arising from the lamellar structure of pure lipoplexes are indicated with asterisks, while the DNA peak is marked by an arrow. Diffraction maxima of hexagonal complexes are indicated with white diamonds and reflections of pure DOPA with black diamonds. For $R < 0.2$, the 1D DNA lattice was diluted, while the lamellar phase was almost unperturbed by DOPA. For $R > 0.2$, DOPA promoted a lamellar-to-hexagonal phase transition of DOTAP−DOPC/DNA that was almost completed at $R \sim 2$, when hexagonal complexes were found to coexist with pure DOPA, forming the cubic phase *Pn*3*m*.

diamonds) were clearly visible in the SAXS patterns of both samples and were indexed as the (10), (11), and (20) reflections of an inverted hexagonal phase with a 64.8 Å structural unit. The lamellar-to-hexagonal phase transition was complete at $R = 1$ in the case of DC-Chol−DOPE/DNA systems, while DOTAP−DOPC/DNA lipoplexes partly resisted solubilization, as shown by the presence of the first-order lamellar Bragg peak (asterisk). At $R = 5$, DC-Chol−DOPE/DNA complexes were almost solubilized, while a major part of the hexagonal DOTAP−DOPC/DNA lipoplexes still coexisted with pure DOPA.

Figure 9 (panel B) shows the phase diagrams of DOTAP−DOPC/DNA/DOPA and DC-Chol−DOPE/DNA/DOPA, with phase regions separated by dashed lines. In the first region (I), only lamellar lipoplexes were detected (lamellar *d* spacings are indicated with black triangles). In the second region (II), lamellar and hexagonal lipoplexes coexisted. The increase of both the lamellar (black triangles) and hexagonal

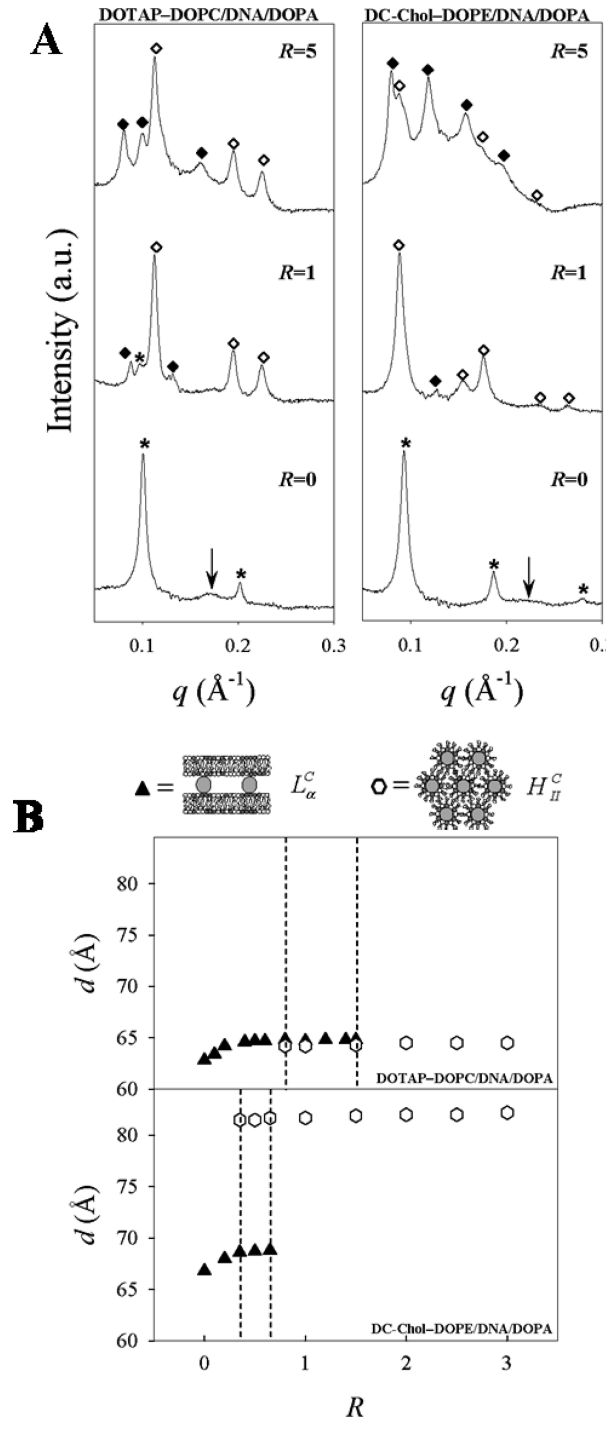

FIGURE 9. Panel A: SAXS patterns of DOTAP−DOPC/DNA and DC-Chol−DOPE/DNA lipoplexes ($\Phi = 0.25$) upon interaction with increasing amounts of DOPA. Bragg peaks arising from the lamellar structure of pure lipoplexes are indicated with asterisks, while the DNA peak is marked by an arrow. Diffraction maxima of hexagonal complexes are indicated with white diamonds and reflections of pure DOPA with black diamonds. Panel B: Phase diagrams of DOTAP−DOPC/DNA and DC-Chol−DOPE/DNA lipoplexes ($\Phi = 0.25$) with differing DOPA contents. Dashed lines separate regions occupied by lamellar lipoplexes, coexisting lamellar and hexagonal lipoplexes, and hexagonal lipoplexes. Repeat spacings, *d*, of lamellar and hexagonal lipoplexes are indicated with black triangles and white hexagons, respectively. To clarify, the *R* range was restricted to 3.5.

(white hexagons) spacings is consistent with the inclusion of DOPA molecules within lipid membranes (4). In the last

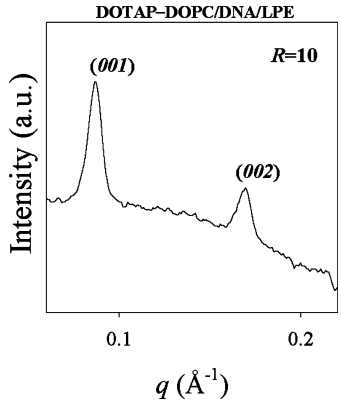

FIGURE 10. SAXS patterns of DOTAP−DOPC/DNA/LPE at $R = 10$. As is evident, a major part of the lamellar phase of lipoplexes resisted solubilization by natural lipid extracts.

region (III), only hexagonal lipoplexes were found to exist. The structure and phase behavior of all lipoplex formulations were found to be intermediate between those of DOTAP−DOPC/DNA/DOPA and DC-Chol−DOPE/DNA/DOPA mixtures.

In conclusion, our SAXS findings on lipoplex/DOPA mixtures show that (i) DOPA holds the potential to promote a lamellar-to-hexagonal phase transition in lamellar lipoplexes, (ii) the anionic/cationic charge ratio at which solubilization of lipoplexes by DOPA is completed, R^*, depends on the lipoplex formulation, (iii) DOPA solubilizes lipoplexes rich in DOPE much more easily than those rich in DOPC, (iv) given a specific lipid composition, lipoplexes of higher membrane charge density (i.e., lower Φ) require lower R ratios to be solubilized by ALs. The latter finding seems to suggest that the stability of the lipoplex structure upon interaction with ALs depends not only on electrostatic issues (i.e., on R) but also on the molar ratio between AL and the total lipid composing the membrane of lipoplexes. This result enforces the general expectation that additional critical factors besides electrostatic interactions in the molecular machinery of lipid-mediated DNA delivery exist.

3.1.4. Structural Evolution of Lipoplexes upon Interaction with Natural Lipid Extracts. Figure 10 shows the SAXS pattern of DOTAP−DOPC/DNA/LPE complexes at $R = 10$. Bragg peaks of the lamellar structure of DOTAP−DOPC/DNA complexes coexisted with pure diffuse scattering because of the form factor of LPE liposomes. Thus, LPE did not perturb the structure of lipoplexes remarkably, with the main effects being essentially two: (i) the lamellar d spacing increased because of the diffusion of ALs within the bilayer of lipoplexes; (ii) the inter-DNA positional correlation was lost, as shown by the vanishing of the "DNA peak" onto the SAXS pattern. At a fixed R value, lipid extracts expressed a much lower ability to destroy the initial lamellar structure of the lipoplexes with respect to pure ALs, MM1, and MM2 independently from the cationic formulations used. According to the results of section 3.1.3, this result is most likely due to the low membrane charge density of LPE, which is roughly 10 times lower than that of pure anionic liposomes.

3.2. Electrophoresis Experiments. The extent of DNA release from different lipoplex formulations after interaction with ALs was investigated by electrophoresis on agarose gels as a function of increasing R. The gel electrophoresis assay allows the determination of the molar fraction of released DNA, X_{DNA}, while other techniques, such as the fluorescence resonance energy-transfer assay, may overestimate DNA release because it includes also DNA that is no longer electrostatically associated with cationic lipids but is still entrapped within the lipid aggregate (33).

3.2.1. DNA-Releasing Capacity of Lipoplexes upon Interaction with DOPG. Figure 11 (panel A) shows the molar fraction of released DNA, X_{DNA}, as a function of the anionic/cationic charge, R. We report the results for DOTAP−DOPC/DNA/DOPG and DC-Chol−DOPE-DMPC/DNA/DOPG mixtures because these systems showed the largest difference in the DNA-releasing ability. We observe that DC-Chol−DOPE−DMPC/DNA complexes display the lowest extent of DNA release, while DOTAP−DOPC/DNA complexes exhibit the largest DNA release. The latter observation is well consistent with our SAXS experiments (Figure 5). These findings support the existence of a general correlation between the structural stability of lipoplexes upon interaction with cellular lipids and DNA unbinding: the lower the complex stability, the higher the DNA release from lipoplexes.

3.2.2. Effect of the Anionic Membrane Charge Density on the DNA-Releasing Capacity of Lipoplexes. Figure 11 (panel B) shows the molar fraction of DNA released, X_{DNA}, as a function of increasing R for DOTAP−DOPC/DNA lipoplexes upon interaction with DOPS and MM2 liposomes. As clearly shown, the molar fraction of DNA released from DOTAP−DOPC/DNA/DOPS is much larger than that released from DOTAP−DOPC/DNA/MM2 complexes, at any R value. These results are in very good agreement with our SAXS experiments reported in Figure 7, which indicate the charge density of the anionic membrane as a key parameter regulating lipoplex destabilization. Electrophoresis experiments therefore point out that the charge density of the anionic membrane controls the DNA-releasing activity of lipoplexes.

3.2.3. Effect of Phase Evolution of Lipoplexes upon Interaction with ALs on Their DNA-Releasing Capacity. Figure 11 (panel C) shows the molar fraction of DNA released, X_{DNA}, from DOTAP−DOPC/DNA lipoplexes ($\Phi = 0.5$) upon interaction with DOPG and DOPA ALs. Figure 11 (panel C) clearly shows that $X_{DNA} \sim 1$ at $R = 5$, therefore suggesting that the DNA-releasing abilities of DOPG and DOPA are comparable in terms of R. This finding most likely suggests that the formation of nonlamellar phases, such as those observed with lipoplex/DOPA mixtures (Figure 8), is not an essential prerequisite for efficient DNA release. However, at $R = 5$, DOTAP−DOPC/DNA lipoplexes were completely destroyed by DOPG (Figure 5, left panel), while they resisted solubilization by DOPA and adopted a hexagonal phase (Figure 8). Combining such observations, we conclude that lamellar phases need complete disintegration to release their DNA cargo, while hexagonal complexes can release DNA even though not entirely solubilized.

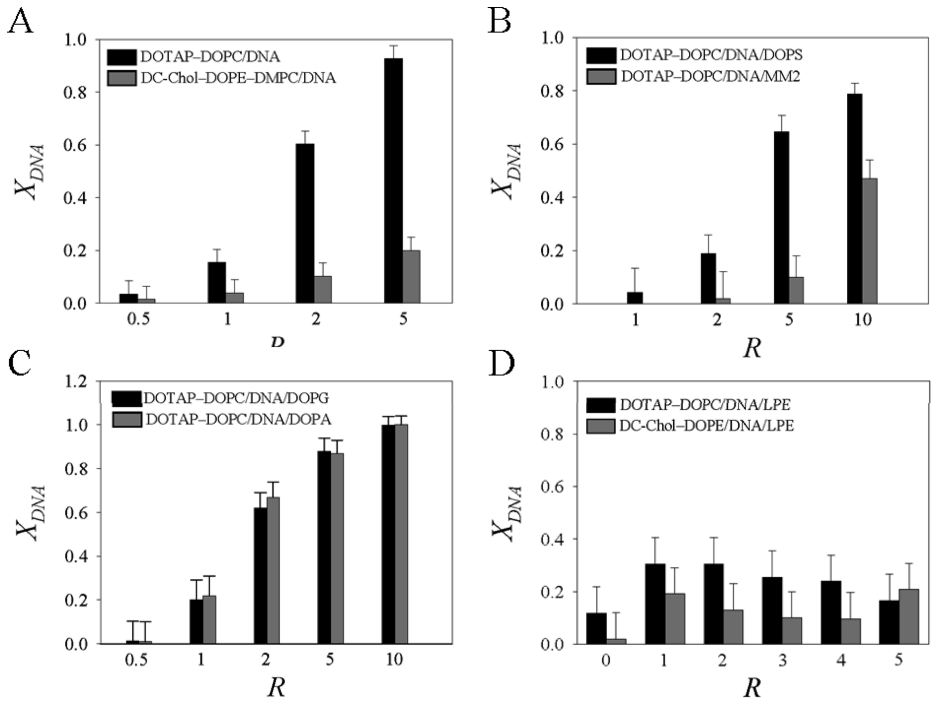

FIGURE 11. Panel A: Molar fraction of DNA released from DOTAP−DOPC/DNA (black histograms) and DC-Chol−DOPE−DMPC/DNA (gray histograms) by DOPG as a function of *R*. Panel B: Molar fraction of DNA released from DOTAP−DOPC/DNA by DOPS (black histograms) and MM2 liposomes (gray histograms) as a function of *R*. Panel C: Molar fraction of DNA released from DOTAP−DOPC/DNA by DOPG (black histograms) and DOPA (gray histograms) as a function of *R*. As is evident, the DNA-releasing efficiencies of the two cellular lipid species are almost the same. Panel D: Molar fraction of DNA released from DOTAP−DOPC/DNA (black histograms) and DC-Chol−DOPE/DNA (gray histograms) by LPE as a function of *R*.

3.2.4. DNA Release from Lipoplexes upon Interaction with Natural Lipid Extracts. Natural lipid extracts turned out to be much less effective in releasing DNA from the lipoplexes than did pure ALs (Figure 11, panel D). Noteworthy is that a new band can be seen just below the wells after the addition of negative natural lipid extracts (see the Supporting Information). We interpret the new band as plasmid DNA, which is released from the lipid surface so that it is available to Et-Br but still confined by cationic AL aggregates so that it cannot migrate very far from the wells. A considerable amount of DNA may remain trapped inside the resultant mesophases: its considerable retardation indicates a large reduction in the negative charge and/or formation of a supramolecular complex.

4. DISCUSSION

The transfection of cells by lipoplexes is a very complex process with a number of different stages (43−46). Several publications have called attention to specific barriers for transfection that may be rate-limiting (47−49). Among these, DNA release from the cationic lipid surroundings is strongly required for gene expression. This process is supposed to be facilitated by ALs of cellular membranes by means of lipid exchange and neutralization of the cationic charge (47). Indeed, cationic lipid−DNA interactions are strong, and the only possibility for release of DNA under cellular conditions seems to be neutralization of the cationic lipid charge with cellular ALs. Thus, intermixing of membrane lipids with lipoplex lipids is presumed to be a necessary step in transfection.

A number of recent findings have shown that the structure of lipoplexes might change dramatically upon mixing with cellular lipids (27, 31, 32) and, furthermore, that such changes may critically affect the DNA delivery efficiency (28, 29). As a result, a viewpoint now emerging is that the critical factor in lipid-mediated transfection is the structural and phase evolution of lipoplexes upon interaction and mixing with cellular lipids.

Here we have reported an analytical study on the interactions between lipoplexes and ALs, negatively charged lipids MM composition, and natural lipid extracts. To facilitate and rationalize the discussion, the following main points will be discussed: (1) the structural evolution of lipoplexes upon interaction with anionic membranes with distinct charge densities and a specific propensity to form either lamellar or nonlamellar phases; (2) the correlation between such an evolution and DNA release.

First, we investigated the structural evolution of seven lipoplex formulations with systematic variations in the headgroup and hydrophobic regions upon interaction with DOPG and DOPS, two ALs common in eukaryotic cells, which are well-known for their tendency to form lamellar phases. Remarkably, two interaction regimes were identified. In the first regime, which we called the "DNA lattice dilution regime", ALs had a minor effect on the nanostructure of lipoplexes, namely, a slight increase in the lamellar *d* spacing and a decrease in the long-range order, as shown by the reduction of the average multilayer domain size, L_m (Figure 3). On the other hand, the 1D DNA packing density was largely affected by ALs. Dilution of the DNA lattice with *R*

was most likely due to diffusion of ALs within the lipoplex bilayer (31, 47). We have identified a threshold ($R = R^{DNA}$; Table 1) from which the correlation between DNA strands was lost; as shown by the vanishing of the "DNA peak" in the SAXS pattern (Figure 3). Even though R^{DNA} was found to be dependent both on the lipoplex and on the ALs, dilution of the DNA lattice at low values of R ($R^* < 1$) was a feature common to all of the investigated lipoplex/AL mixtures. It is currently believed that in cells lipoplexes may interact with a number of cellular membranes and that DNA may be gradually released after a number of multiple interactions. The physical meaning of our results is therefore that dilution of the 1D DNA lattice occurs at the early stages of interaction. We underline that our SAXS results are the first data reported in the literature showing such a clear dilution of the 1D DNA lattice of lipoplexes promoted by anionic cellular lipids.

In the second stage, the structure of lipoplexes was disintegrated by ALs. The structural stability of lipoplexes upon interaction with ALs was strictly dependent on the lipoplex lipids, as is clearly shown in Figure 5. Therefore, it was possible to define for each lipoplex formulation a specific R^*, the anionic/cationic charge ratio at which lipoplex disintegration is completed (Table 1). To better interpret these results, we applied agarose gel electrophoresis experiments to estimate the percentage of released DNA by lipoplexes upon interaction with ALs. Figure 11 (panel A) shows that the extent of DNA release estimated by electrophoresis does correlate with the structural stability of the lipoplexes, as revealed by synchrotron SAXS. For instance, in the case of DOTAP−DOPC/DNA lipoplexes, completion of DNA release (Figure 11, panel A) occurred close to $R \sim 5$. This value is in very good agreement with R^*, as determined by SAXS (Figure 5). We observe that the most unstable lipoplexes (DOTAP−DOPC/DNA) rapidly release DNA, while the most stable complexes (DC-Chol−DOPE−DMPC/DNA) exhibit a lower extent of DNA release. Therefore, the results can be generalized as follows: the higher the structural stability, the lower the extent of DNA release.

Interaction between oppositely charged membranes of lipoplexes and cells necessarily involves some local contact (50). As a result, the charge densities of lipoplexes and anionic liposomes are expected to play a key role in membrane interaction, contact, fusion (51), and DNA release. To address this issue, we investigated the structural changes of lipoplexes and the simultaneous DNA release upon interaction with several anionic membranes whose charge densities are in the following order: pure ALs > MM1 > MM2 > LPE. SAXS experiments performed on lipoplexes upon interaction with pure DOPG were compared with those obtained with MM1. The latter is a DOPG-containing lipid mixture with a membrane charge density lower than that of pure DOPG (negatively charged lipid constitutes ~30% of the total lipid). As a general rule, dilution of the DNA lattice and disintegration by MM1 occurred at higher R values than those needed when using pure DOPG. Very similar findings were obtained using DOPS and MM2, a DOPS-containing lipid blend with lower membrane charge density (Figure 7). Natural lipid extracts of lower membrane charge density (negatively charged lipid constitutes only 10% of the natural blend) had a minor effect on the structure of lipoplex up to high values of R (Figure 10) and were the weakest DNA releasers (Figure 11, panel D). The latter finding means that natural lipid extracts have less capacity to neutralize the positive charge of the lipoplex lipids most likely because of their much lower charge density. Noteworthy was therefore to infer a very general behavior of lipoplex/AL mixtures from experimental data: the higher the membrane charge density of the anionic membranes, the higher the destabilization of the lipoplex structure (Figures 6, 7, and 10) and the molar fraction of DNA released (Figure 11).

Recent experiments (27−32) have investigated the correlation between the lipoplex phase evolution and DNA release. However, although the phase preferences of the anionic/cationic lipid mixtures might well be expected to influence the DNA-releasing efficiency, the existence of a direct general correlation still remains controversial. To investigate the phenomenon, we used DOPA, a cellular lipid common in eukaryotic cells that is well-known for its nonlamellar phase tendency (52, 53). Interestingly, the existence of a "1D DNA dilution regime" was found (Figure 8; $R^{DNA} \sim 0.5$), confirming that this is a very general feature of lipoplex/AL mixtures at low R. Upon a further increase in R, all of the lipoplex formulations used in the present study exhibited a lamellar−hexagonal phase change, with transition rates depending on the lipoplex composition. This can be seen in Figure 9 (panel B), showing that the extension of the monophasic and biphasic regions of the phase diagram of lipoplex/DOPA mixtures largely depended on the lipid composition.

On the whole, DOPA holds the potential to solubilize lipoplexes rich in DOPE much more easily than those rich in PCs. Conversely, DOPG and DOPS do express a greater ability to destroy the initial structure of complexes rich in PCs. Because DOPE has a negative natural curvature, while PCs are bilayer-forming lipids (for which the curvature is zero), we put forth the concept that ALs with a disposition to form nonlamellar phases (such as DOPA) solubilize more easily complexes made of lipids prone to form nonlamellar structures, while ALs with a tendency to form lamellar phases (such as DOPG and DOPS) express a greater ability to destroy the initial lamellar structure of lipoplexes rich in bilayer-forming lipids.

Such a general feature of lipoplex/AL mixtures suggests that the propensity of lipoplexes to be destroyed by ALs does specifically depend on the shape coupling between lipoplex and anionic membrane lipids. The lipid shape is a very convenient concept, frequently used to describe the volume occupied by phospholipids (54−56). Using this approach, phospholipids can be classed as cylinders (e.g., PC), cones (e.g., PE), and inverted cones (e.g., lysophosphatiodylcholine), depending on the relative volumes of their polar headgroups and fatty acyl chains (57−59). The supramolecular organization, or packing, of such molecules originates

from the widespread bilayer (or lamellar) structure and the nonlamellar (tubular micelles) H_I and H_{II} phases. Among other possible contributions, the influence of the shape and packing constraints on lipid mixing and membrane fusion in lipids appears to be determinant (57−59) even if not deeply understood yet. Despite that, some significant experimental reports have appeared recently that suggest that the low packing competition between lipids generally leads to facilitated mixing and fusion (60−62). According to such studies, our findings are most likely to indicate that a low packing competition between lipoplex and ALs may result in the high incorporation efficiency of ALs within lipoplex membranes. Such a packing-dependent integration ability of ALs is therefore supposed to regulate the destabilization of the lipoplex structure. For instance, a recent study (63) has shown that the ability of a lipid perturbant to compensate for lipid-packing mismatch, that is, to lower the "void" energy, must be taken into account to explain the ability of lipid perturbants to promote stalk formation, which is the commonly recognized initial fusion intermediate that leads to lamellar−hexagonal phase transition. According to such evidence, our hypothesis, based on the "molecular shape" coupling between lipoplex and ALs, most likely explains the ability of conelike ALs (with intrinsic nonzero curvature) to facilitate the compositionally driven lamellar−nonlamellar phase transformations from a complementary point of view (54−63). Cationic DOTAP and DC-Chol as well as neutral DOPC have a cylindrical shape with a cross-sectional area of headgroups approximately equal to the hydrophobic chain area. Thus, they tend to self-assemble into lamellar structures with spontaneous curvature $C_0 = 1/R_0 = 0$. On the other side, DOPE and DOPA, because of their conelike molecular arrangement, give rise to a negative natural curvature and form inverted hexagonal phases. Furthermore, it is well established that the shape of the lipid molecules determines the curvature of the membrane and the structure of the self-assembly. Upon insertion of DOPA within the lipoplex membrane, a large lipid mixing occurs (35). Such a mixing gradually increases the relative molar percentage of conelike lipids in the emerging lipid bilayer with respect to pure lipoplex membranes, and the hexagonal phase becomes favored with respect to the lamellar one. Lipid mixing upon AL inclusion is therefore supposed to induce the compositionally driven lamellar-to-hexagonal phase transition by controlling the spontaneous curvature of the emerging membranes. In summary, lipids that are close in terms of "molecular shape" (such as DOPA and DOPE) appear to have an enhanced ability to mix, therefore lowering the lamellar−nonlamellar phase transition energetic barriers (64).

Recently, it has been suggested that the DNA-releasing capacity of the ALs does correlate with the interfacial curvature of the mesomorphic structures developed when the anionic and CLs are mixed. The preference of the mixed lipid membranes to adopt nonlamellar phases has been suggested as a key factor for the rate and extent of DNA release (27−30, 44, 46). However, our electrophoretic results say exactly the opposite. For example, Figure 11 (panel C) clearly shows that DNA was almost completely released from DOTAP−DOPC/DNA lipoplexes by DOPG and DOPA almost at the same value of R ($R \sim 5$). Therefore, ALs forming highly curved phases are not the better DNA-releasing agents. Thus, we propose that the characteristics of the ALs in terms of their efficiency of DNA release may only be meaningful in the context of specific lipoplexes.

On the other hand, SAXS experiments showed that lipoplex/DOPA mixtures underwent lamellar-to-hexagonal phase transition, while lipoplex/DOPG mixed systems did not. Thus, our findings suggest that the formation of nonlamellar phases does not universally correlate with higher DNA release (28−30). However, if the DNA-releasing abilities of DOPG and DOPA are definitely comparable in terms of R, their abilities to destroy the structure of lipoplexes were clearly different, as discussed above. Indeed, at $R = 5$, DOTAP−DOPC/DNA lipoplexes were completely solubilzed by DOPG (Figure 5, left panel), while they resisted solubilization by DOPA and adopted a hexagonal phase (Figure 8). Combining such observations, we conclude that lamellar phases need complete disintegration to release their DNA cargo, while hexagonal complexes can release DNA even though not entirely solubilized.

In summary, a correlation between the releasing capacities of the ALs and the mesomorphic structures that they form when mixed with the cationic lipoplex lipids was not found in our experiments. This observation most likely indicates that the formation of nonlamellar phases, such as those observed with lipoplex/DOPA mixtures (Figure 8), is not an essential prerequisite for efficient DNA release. However, our data are not in contradiction with those previously reported (27−30) but enforce our suggestion that the phase evolution of lipoplexes upon interaction with cellular ALs as well as DNA release is strongly dependent on the lipid composition of both lipoplexes and anionic membranes (Figure 12).

Numerous contacts visualized by electron microscopy between lipoplexes and various cellular membranes (65) seem to support a concept of gradual lipoplex peeling and DNA release. Given the need for intermixing of the membrane lipids with the lipoplex lipids, our findings take on a particular significance because the ability of ALs to initiate DNA release could depend on the extent of membrane fusion (strictly, lipid mixing) between anionic liposomes and lipoplexes, which, in turn, may be regulated by shape coupling between lipoplex and anionic membrane lipids.

The approach presented here emphasizes the importance of the lipid composition of both lipoplexes and target membranes. A growing amount of evidence shows that nonbilayer structures with relevance in the processes of fusion and fission of lipid bilayers can occur in some types of biological membranes (e.g., endoplasmic reticulum, inner mitochondrial membrane, prolamellar bodies). Indeed, we emphasize that, when a correlation between the mechanisms of gene transfection and the phase behavior of lipid gene vectors is established, desired mesophases may ratio-

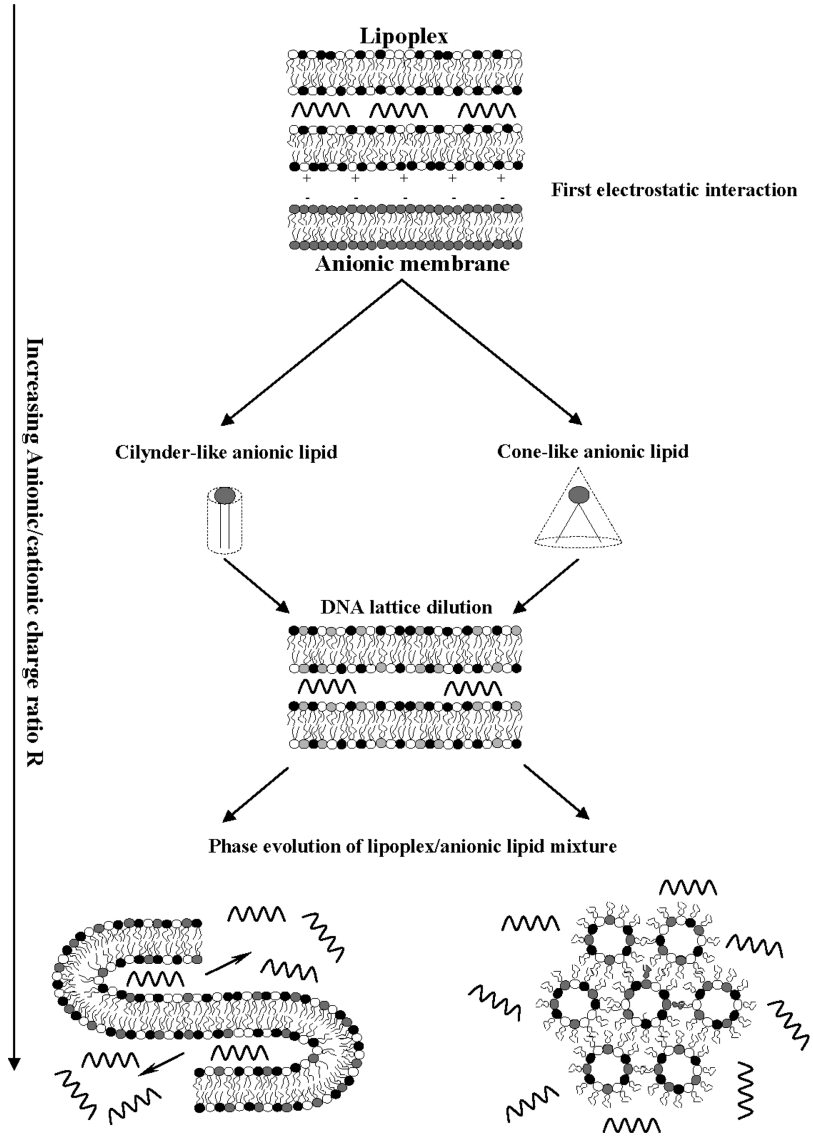

FIGURE 12. Schematic presentation of the phase evolution of lipoplexes after interaction with anionic membranes. The very first electrostatic interaction promotes the local interaction and fusion of lipoplex and anionic membranes. At the early stages of interaction, some ALs diffuse within the lipoplex bilayer, the main effects being a weaking of the cationic lipid/DNA interaction and dilution of the 1D DNA lattice. Upon further interaction, the lipoplex phase behavior comes to depend on the molecular shape of the lipids composing anionic membranes. Phase transition rates and the efficiency of DNA release are strongly dependent on the shape coupling between lipoplexes and ALs.

nally be obtained by adapting the lipoplex composition to the lipid composition of the target membranes of cells to be transfected.

5. CONCLUSIONS

We have provided new insight into the mechanism of the structural and phase evolution of lipoplexes upon interaction and mixing with anionic cellular lipids. For the first time, the universal behavior of lipoplex/AL mixtures at low anionic/cationc charge ratios was demonstrated. Dilution of the 1D DNA lattice, as determined by synchrotron SAXS, is unambiguous proof of the mechanism of charge neutralization of cationic lipids by anionic membranes (23, 24). Upon further interaction, disintegration of lipoplexes by ALs as well as the formation of nonlamellar phases in lipoplex/AL mixtures is strongly affected by the shape coupling between lipoplexes and ALs. Furthermore, coupling between the membrane charge densities of lipoplexes and anionic membranes plays a major role in regulating the evolution of lipoplex/AL mixtures and the release of plasmid DNA. These results highlight the phase properties of the carrier lipid/cellular lipid mixtures as a decisive factor for transfection success and strengthen the concept that the structural evolution of lipoplexes upon interaction with cellular lipids appears to be a controlling factor in DNA release and, in turn, in lipid-mediated DNA delivery.

Acknowledgment. Dr. T. Narayanan and Dr. E. Di Cola of the experimental staff of ID02 at the European Synchrotron Radiation Facility (ESRF, Grenoble, France) are gratefully acknowledged.

Supporting Information Available: Digital photograph of DOTAP-DOPC/DNA and DC-Chol-DOPE/DNA lipoplexes upon mixing with increasing LPE. Mixed systems were prepared with increasing anionic/cationic molar ratios: $R = 0$ (lane a), $R = 1$ (lane b), $R = 2$ (lane c), $R = 3$ (lane d), $R = 4$ (lane e),

$R = 5$ (lane f), and control DNA (lane g). Experiments revealed two major bands for naked DNA (lane g). The high-mobility band was attributed to the most compact (supercoiled) form, and the less-intense one was considered to be the nonsupercoil content in the plasmid preparation. This material is available free of charge via the Internet at http://pubs.acs.org.

REFERENCES AND NOTES

(1) Felgner, P. L.; Ringold, G. M. *Nature* **1989**, *337*, 387–388.
(2) Miller, A. D. *Curr. Med. Chem.* **2003**, *10*, 1195–1211.
(3) Dan, N. *Biophys. J.* **1997**, *73*, 1842–1846.
(4) Bruinsma, R.; Mashl, J. *Europhys. Lett.* **1998**, *41*, 165–170.
(5) Bruinsma, R. *Eur. Phys. J. B* **1998**, *4*, 75–88.
(6) Dan, N. *Biochim. Biophys. Acta* **1998**, *1369*, 34–38.
(7) Harries, D.; May, S.; Gelbart, W. M.; Ben-Shaul, A. *Biophys. J.* **1998**, *75*, 159–173.
(8) May, S.; Harries, D.; Ben-Shaul, A. *Biophys. J.* **2000**, *78*, 1681–1697.
(9) May, S.; Ben-Shaul, A. *Curr. Med. Chem.* **2004**, *11*, 1241–1253.
(10) Farago, O.; Grønbech-Jensen, N.; Pincus, P. *Phys. Rev. Lett.* **2006**, *96*, 018102.
(11) Rädler, J. O.; Koltover, I.; Salditt, T.; Safinya, C. R. *Science* **1997**, *275*, 810–814.
(12) Koltover, I.; Salditt, T.; Rädler, J. O.; Safinya, C. R. *Science* **1998**, *281*, 78–81.
(13) Koltover, I.; Salditt, T.; Safinya, C. R. *Biophys. J.* **1999**, *77*, 915–924.
(14) Caracciolo, G.; Pozzi, D.; Caminiti, R.; Congiu Castellano, A. *Eur. Phys. J. E* **2003**, *10*, 331–336.
(15) Dias, R. S.; Lindman, B.; Miguel, M. G. *J. Phys. Chem. B* **2002**, *106*, 12600–12607.
(16) Dias, R.; Antunes, F.; Miguel, M.; Lindman, S.; Lindman, B. *Braz. J. Med. Biol. Res.* **2002**, *35*, 509–522.
(17) Gonçalves, E.; Debs, R. J.; Heath, T. D. *Biophys. J.* **2004**, *86*, 1554–1563.
(18) Cárdenas, M.; Campos-Terán, J.; Nylander, T.; Lindman, B. *Langmuir* **2004**, *20*, 8597–603.
(19) McManus, J. J.; Rädler, J. O.; Dawson, K. A. *J. Am. Chem. Soc.* **2004**, *126*, 15966–15967.
(20) Alfredsson, V. *Curr. Opin. Colloid Interface Sci.* **2005**, *10*, 269–273.
(21) Milani, S.; Bombelli, F. B.; Berti, D.; Baglioni, P. *J. Am. Chem. Soc.* **2007**, *129*, 11664–11665.
(22) Leal, C.; Moniri, E.; Pegado, L.; Wennerström, H. *J. Phys. Chem. B* **2007**, *111*, 5999–6005.
(23) Banchelli, M.; Betti, F.; Berti, D.; Caminati, G.; Bombelli, F. B.; Brown, T.; Wilhelmsson, L. M.; Nordén, B.; Baglioni, P. *J. Phys. Chem. B* **2008**, *112*, 10942–10952.
(24) Lundqvist, M.; Stigler, J.; Elia, G.; Lynch, I.; Cedervall, T.; Dawson, K. A. *Proc. Natl. Acad. Sci. U.S.A.* **2008**, *105*, 14265–14270.
(25) Henriques, A. M.; Madeira, C.; Fevereiro, M.; Prazeresa, D. M. F.; Aires-Barrosa, M. R.; Monteiro, G. A. *Int. J. Pharm.* **2009**, *377*, 92–98.
(26) Rao, N. M.; Gopal, V. *Biosci. Rep.* **2006**, *26*, 301–324.
(27) Yury, S.; Tarahovsky, Y.; Koynova, R.; MacDonald, R. C. *Biophys. J.* **2004**, *87*, 1054–1064.
(28) Koynova, R.; Wang, L.; Tarahovsky, Y.; MacDonald, R. C. *Bioconjugate Chem.* **2005**, *16*, 1335–1339.
(29) Koynova, R.; Wang, L.; MacDonald, R. C. *Proc. Natl. Acad. Sci. U.S.A.* **2006**, *103*, 14373–14378.
(30) Koynova, R.; MacDonald, R. C. *Biochim. Biophys. Acta* **2007**, *1714*, 63–70.
(31) Caracciolo, G.; Marchini, C.; Pozzi, D.; Caminiti, R.; Amenitsch, H.; Montani, M.; Amici, A. *Langmuir* **2007**, *23*, 4498–4508.
(32) Caracciolo, G.; Pozzi, D.; Caminiti, R.; Marchini, C.; Montani, M.; Amici, A.; Amenitsch, H. *Appl. Phys. Lett.* **2007**, *91*, 143903.
(33) Wang, L.; Koynova, R.; Parikh, H.; MacDonald, R. C. *Biophys. J.* **2006**, *91*, 3692–3706.
(34) Pozzi, D.; Amenitsch, H.; Caminiti, R.; Caracciolo, G. *Chem. Phys. Lett.* **2006**, *422*, 439–445.
(35) Caracciolo, G.; Pozzi, D.; Amenitsch, H.; Caminiti, R. *Langmuir* **2005**, *21*, 11582–11587.
(36) Caracciolo, G.; Pozzi, D.; Amenitsch, H.; Caminiti, R. *Appl. Phys. Lett.* **2005**, *87*, 133901.
(37) Caracciolo, G.; Pozzi, D.; Caminiti, R.; Amenitsch, H. *J. Phys. Chem. B* **2006**, *110*, 20829–20835.
(38) Marchini, C.; Montani, M.; Amici, A.; Pozzi, D.; Caminiti, R.; Caracciolo, G. *Appl. Phys. Lett.* **2009**, *94*, 033903.
(39) Caracciolo, G.; Pozzi, D.; Caminiti, R.; Marchini, C.; Montani, M.; Amici, A.; Amenitsch, H. *Biochim. Biophys. Acta* **2007**, *1768*, 2280–2292.
(40) Amenitsch, H.; Rappolt, M.; Kriechbaum, M.; Mio, H.; Laggner, P.; Bernstorff, S. *J. Synchrotron Radiat.* **1998**, *5*, 506–508.
(41) Boesecke, P. *J. Appl. Cryst.* **2007**, *40*, 423—427.
(42) Salditt, T.; Koltover, I.; Rädler, J. O.; Safinya, C. R. *Phys. Rev. E* **1998**, *58*, 889–904.
(43) Friend, D. S.; Papahadjopoulos, D.; Debs, R. J. *Biochim. Biophys. Acta* **1996**, *1278*, 41–50.
(44) Zuhorn, I. S.; Kalicharan, R.; Hoekstra, D. *J. Biol. Chem.* **2002**, *277*, 18021–18028.
(45) Elouahabi, A.; Ruysschaert, J.-M. *Mol. Ther.* **2005**, *11*, 336–347.
(46) Hoekstra, D.; Rejman, J.; Wasungu, L.; Shi, F.; Zuhorn, I. *Biochem. Soc. Trans.* **2007**, *35*, 68–71.
(47) Xu, Y. H.; Szoka, F. C. *Biochemistry* **1996**, *35*, 5616–5623.
(48) Zelphati, O.; Szoka, F. C. *Proc. Natl. Acad. Sci. U.S.A.* **1996**, *93*, 11493–11498.
(49) Cornelis, S.; Vandenbranden, M.; Ruysschaert, J. M.; Elouahabi, A. *DNA Cell. Biol.* **2002**, *21*, 91–97.
(50) Pantazatos, D. P.; Pantazatos, S. P.; MacDonald, R. C. *J. Membr. Biol.* **2003**, *194*, 129–139.
(51) Hed, G.; Safran, S. A. *Phys. Rev. Lett.* **2004**, *93*, 138101.
(52) Hafez, I. M.; Ansell, S.; Cullis, P. R. *Biophys. J.* **2000**, *79*, 1438–1446.
(53) Kooijman, E. E.; Carter, K. M.; van Laar, E. G.; Chupin, V.; Burger, K. N. J.; de Kruijff, B. *Biochemistry* **2005**, *44*, 17007–17015.
(54) Israelachvili, J. N.; Mitchell, D. J.; Ninham, B. W. *J. Chem. Soc.* **1976**, *72*, 1525–1568.
(55) Cavagnetto, F.; Relini, A.; Mirghani, Z.; Gliozzi, A.; Bertoia, D.; Gambarcorta, A. *Biochim. Biophys. Acta* **1992**, *1106*, 273–281.
(56) Kleinfeld, A. M. In *Membrane Fusion*; Wilschut, J., Hoeckstra, D., Eds.; Dekker: Groningen, The Netherlands, 1990; pp 3—33.
(57) Kumar, V. V. *Proc. Natl. Acad. Sci. U.S.A.* **1991**, *88*, 444–448.
(58) Marsh, D. *Biophys. J.* **1996**, *70*, 2248–2255.
(59) Escribá, P. V.; Ozaita, A.; Ribas, C.; Miralles, A.; Fodor, E.; Farkas, T.; García-Sevilla, J. A. *Proc. Natl. Acad. Sci. U.S.A.* **1997**, *94*, 11375–11380.
(60) Funari, S. S.; Barceló, F.; Escribá, P. V. *J. Lipid Res.* **2003**, *44*, 567–575.
(61) Megha Bakht, O.; London, E. *J. Biol. Chem.* **2006**, *281*, 21903–21913.
(62) Risselada, H. J.; Marrink, S. J. *Phys. Chem. Chem. Phys.* **2009**, *11*, 2056–2067.
(63) Haque, M. D. E.; Lentz, B. R. *Biochemistry* **2004**, *43*, 3507–3517.
(64) Kasson, P. M.; Pande, V. S. *PLoS Comput. Biol.* **2007**, *3*, e220.
(65) Koynova, R.; Tarahovsky, Y.; Wang, L.; MacDonald, R. C. *Biochim. Biophys. Acta* **2007**, *1768*, 375–386.

AM900406B